Electrically Powered Locomotion of Dual-Nature Colloid-Hedgehog and Colloid-Umbilic Topological and Elastic Dipoles in Liquid Crystals

Bohdan Senyuk, Richmond E. Adufu, and Ivan I. Smalyukh*

Read Online

| ACCESS | Metrics & More | Article Recommendations | SI Supporting Information |

ABSTRACT: Colloidal particles in liquid crystals tend to induce topological defects and distortions of the molecular alignment within the surrounding anisotropic host medium, which results in elasticity-mediated interactions not accessible to their counterparts within isotropic fluid hosts. Such particle-induced coronae of perturbed nematic order are highly responsive to external electric fields, even when the uniformly aligned host medium away from particles exhibits no response to fields below the realignment threshold. Here we harness the nonreciprocal nature of these facile electric responses to demonstrate colloidal locomotion. Oscillations of the electric field prompt repetitive deformations of the corona of dipolar elastic distortions around the colloidal inclusions, which upon appropriately designed electric driving synchronize the displacement directions. We observe the colloid-hedgehog dipole accompanied by an umbilical defect in the tilt directionality field (**c**-field), along with the texture of elastic distortions that evolves with a change in the applied voltage. The temporal out-of-equilibrium evolution of the director and **c**-field distortions around particles when the voltage is turned on and off is not invariant upon reversal of time, prompting lateral translations and interactions that markedly differ from those accessible to these colloids under equilibrium conditions. Our findings may lead to both technological and fundamental science applications of nematic colloids as both model reconfigurable colloidal systems and as mesostructured materials with predesigned temporal evolution of structure and composition.
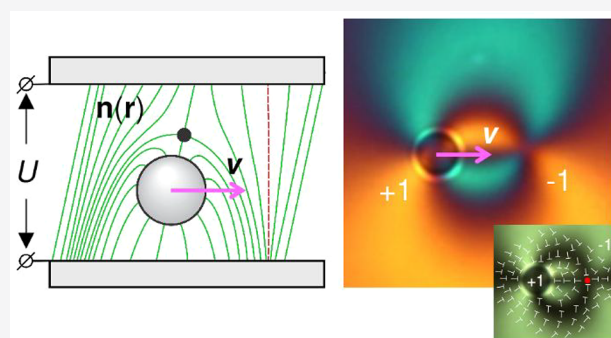
■ INTRODUCTION

Synthetic systems made of active or externally driven components have opened new perspectives for the design and applications of materials. Colloidal and liquid crystal (LC) systems are examples of soft matter that often exhibit stark structural similarities with the forms of molecular and colloidal self-organization found in living organisms, but they are most commonly studied under equilibrium conditions.[1,2] Manipulation and motion of individual colloidal particles or microswimmers and their ensembles in different host media self-propelled or controlled by means of chemical, thermal, electrical, or other external stimuli attract a great deal of attention due to the possible new ways of assembly, microfluidic transport, and the variety of their collective dynamics reminiscent of schooling and flocking among living organisms, the active matter.[3–9] LCs as a host for such driven colloidal systems introduce another level of complexity due to the anisotropy of their physical properties with respect to the director field $\mathbf{n(r)} \equiv -\mathbf{n(r)}$ describing the locally averaged spatial patterns of orientation of LC molecules. This complexity is accompanied by a variety of new possibilities and means of directing the motion of colloidal microswimmers with an increased level of control due to the facile response of

LC molecules to external stimuli such as magnetic, optical, or electric fields.[10–12] Colloidal dynamics in LCs exhibit a rich diversity of physical phenomena,[13] and recently, a number of studies explored the electrically driven transport of colloidal particles[13–19] and particle-like topological solitons[8,9,20] in LCs.

Here we focus on electrically driven directional locomotion of artificial microswimmers formed by elastic colloidal dipoles[21–24] in nematic LCs. We show that electrically driven propulsion of elastic dipoles in a strongly confined LC results from the nonreciprocal director dynamics that can be also understood in terms of complex elastic interactions between colloidal particles and induced nonsingular umbilical defects that are reconfigured by voltage. We observe that upon application of an electric field, the uniaxial colloid-hedgehog dipole[21,22,24] is accompanied by an additional umbilical defect in the $\mathbf{n(r)}$ tilt directionality field (the **c**-field) forming a field-
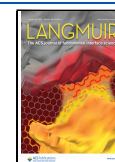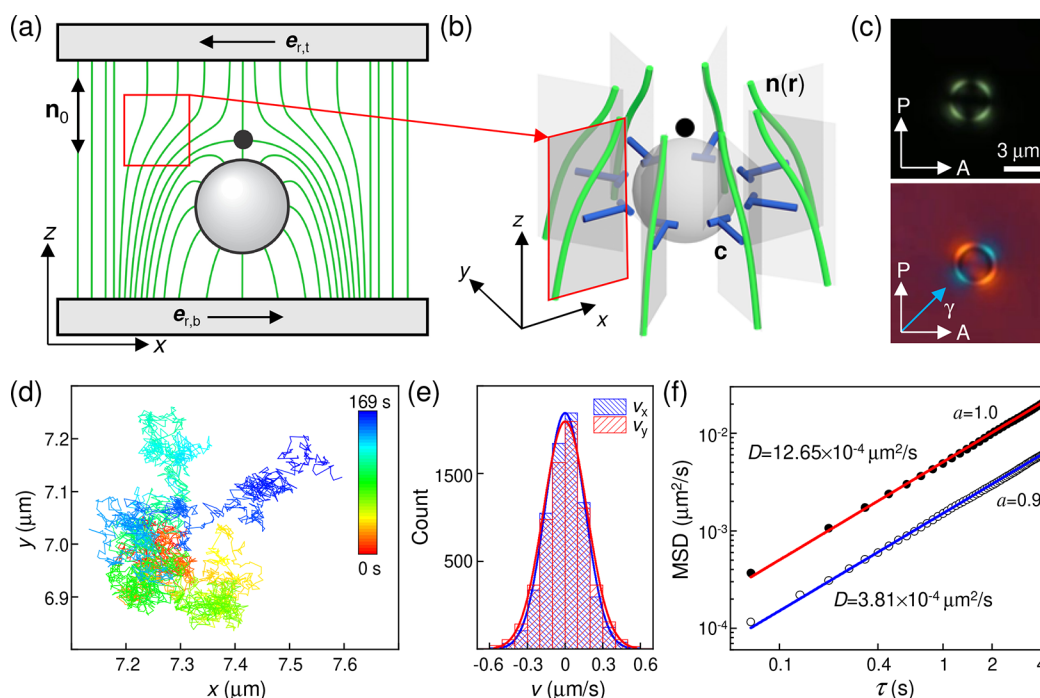
Figure 1. Elastic dipoles in a homeotropic nematic cell. (a) Schematic of a director field (green lines) around an elastic dipole in a homeotropic cell; $\mathbf{e}_{r,t}$ and $\mathbf{e}_{r,b}$ show the directions of weak rubbing of the top and bottom confining substrates, respectively, coated with alignment films. Note that the schematic is not to scale as the particle diameter in our experiments constitutes ∼60% of the cell thickness. (b) Definition of a polar vector **c** (blue nails), which is a projection of a tilted director $\mathbf{n}(\mathbf{r})$ on the $x-y$ plane. The LC-embedded SP with perpendicular anchoring induces a radial two-dimensional tilt directionality **c** vector field with a radial orientation close to the particle. (c) Polarizing microscopy textures of an elastic dipole in a homeotropic cell. (d) Example of a trajectory of SP undergoing Brownian motion in the plane of a homeotropic cell. (e) Histograms of velocities during displacements in the plane of a cell along the x and y directions. (f) Log−log plots of mean-square displacement (MSD) as a function of lag time measured for SP in a homeotropic cells with thicknesses d of 5.5 mm (blue fitting line) and 10 μm (red fitting line). Experimental data were fitted using the expression[1] MSD = $4D\tau^a$, where $a \approx 1$, which indicates normal diffusion of SPs due to random Brownian motion.

induced biaxial nematostatic dipole.[25,26] We describe how oscillations of a specially designed low-frequency electric field cause repetitive transformation of director distortions around the colloidal inclusion, and this temporal out-of-equilibrium evolution of the LC director and **c**-field distortions around particles when the voltage is turned on and off is not invariant upon reversal of time, prompting lateral locomotion of the colloidal particles. Our findings provide new insights into the phenomenological richness of colloids in LCs in terms of their controlled manipulation, assembly, and collective dynamics.

EXPERIMENTAL SECTION

Materials. We used a room-temperature nematic LC ZLI-2806 (EMD Electronics) as a host medium for colloidal particles. To obtain elastic dipoles, we used silica spheres with a diameter $2R_0 = 3.14$ μm (Duke Scientific) treated with an aqueous solution (0.05 wt %) of N,N-dimethyl-N-octadecyl-3-aminopropyl-trimethoxysilyl chloride (DMOAP) for homeotropic surface boundary conditions. Dilute colloidal dispersions were obtained by dispersing particles in a LC host either via solvent exchange or via mechanical mixing. Particles were dispersed in a nematic LC at a low density of ∼10^5 mm^{-3}, which allows observation of an isolated particle in the field of view with a 100× objective. Colloidal dispersions in a LC state were filled into LC cells after sonication for ∼5 min to break apart preexisting aggregates. LC cells were assembled using glass substrates with transparent indium tin oxide (ITO) electrodes facing inward to allow application of an electric field between opposite substrates. To minimize spherical aberrations in experiments involving high-numerical aperture (NA) oil immersion objectives, one of the two substrates was 0.15−0.17 mm thick (SPI Supplies). Homeotropic surface boundary conditions

at confining substrates were set by thin films of spin-coated and cross-linked polyimide SE1211 (Nissan Chemical Industries, Ltd.). To break the azimuthal degeneracy of the director's tilt during switching of homeotropically aligned nematic ZLI-2806 with a negative dielectric anisotropy $\Delta\varepsilon = -4.8$, SE1211-coated substrates were rubbed once or twice with a velvet cloth applying a weak pressure of ∼380 Pa along a direction $\mathbf{e}_r$ (Figure 1a). Substrates with rubbed alignment layers were assembled in an antiparallel fashion so that $\mathbf{e}_{r,t}$ and $\mathbf{e}_{r,b}$ on the top and bottom substrates, respectively, were parallel but pointing in opposite directions (Figure 1a). A cell gap thickness d ≈5.5 μm was set by glass spacers (Duke Scientific) dispersed in ultraviolet-curable glue (Norland Products, Inc.).

Methods and Techniques. Analog function generator GW Instek GFG-8216A or a data acquisition board (NIDAQ-6363, National Instruments) and homemade MATLAB-based software were used to generate different driving schemes and waveforms of voltage applied to the LC. The latter was used to obtain waveforms of low-frequency voltage with a high carrier frequency f_c of 1 kHz. A high carrier frequency was used to avoid effects associated with the transport of ions at low-frequency applied electric fields. The homemade software allowed us to tune various parameters of applied voltage, and generated waveforms were controlled using a Tektronix TDS 2002B oscilloscope. A threshold voltage U_{th} of 1.84 V$_{p-p}$ of the Fréedericksz transition for a pure ZLI-2806 in homeotropic cells was experimentally determined from the dependence of the capacitance of the cell on the applied voltage measured at 1.0 kHz using a Schlumberger 1260 impedance gain-phase analyzer.

An experimental setup assembled around an inverted Olympus IX81 microscope was used for optical bright-field and polarizing microscopy observations with 20× (NA = 0.4) and oil 100× (NA = 1.4) objectives. The dynamics of LC textures and translational motion of colloids was recorded using a charge-coupled device (CCD)
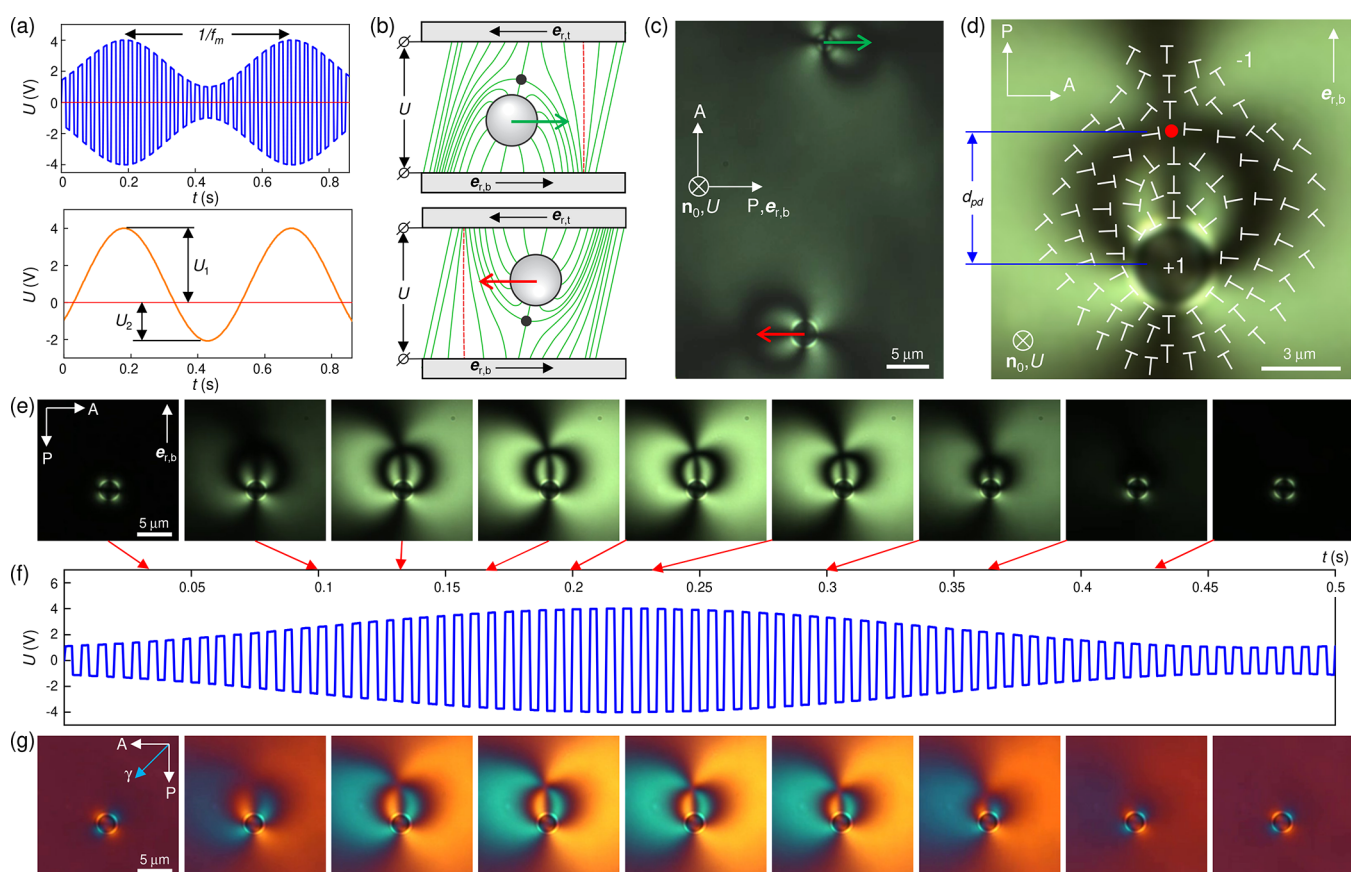
Figure 2. Locomotion of elastic dipoles in a homeotropic nematic cell. (a) Waveforms of an applied voltage U. (b) Schematic of a director field around two elastic dipoles moving in different directions in panel c. Note that the schematic is not to scale as the particle diameter in our experiments constitutes ∼60% of the cell thickness. (c) Polarizing microscope texture around two elastic dipoles moving under an applied voltage U in different directions. (d) Schematic of a **c**-field around an elastic dipole and umbilic defect under an applied voltage. (e−g) Sequences of polarizing microscope textures around an elastic dipole obtained without (e) and with (g) a retardation plate changing with respect to an applied voltage with f_m = 2 Hz and f_c = 1 kHz (f). For the purpose of demonstration, a carrier signal in panel f is represented by a lower frequency.

camera (Flea, PointGrey) at rates of 15 and 30 frames per second, and the exact spatial positions of colloidal spheres as a function of time were then determined from captured video using motion tracking plugins of ImageJ (freeware from the National Institutes of Health) analyzing software.

RESULTS AND DISCUSSION

Colloid-Hedgehog Elastic Dipole in a Homeotropic Nematic Cell. Elastic dipoles with a point defect called a hedgehog were obtained by mixing silica spherical particles (SPs) with homeotropic boundary conditions in a nematic LC and filling the resulting dispersion into a homeotropic LC cell (Figure 1a) with a thickness $d \approx 5.5$ μm, which is slightly larger than the diameter $2R_0 = 3.14$ μm of colloidal particles. The dipolar configuration of the director $\mathbf{n}(\mathbf{r})$ around SPs[22] results from the mismatch of the preset far-field director $\mathbf{n}_0$ in the LC cell and the alignment of LC molecules at the particle's surface with homeotropic conditions. As one can see from the schematic representation of $\mathbf{n}(\mathbf{r})$ in Figure 1a, SP is topologically equivalent to a radial hedgehog defect with a topological charge $s = +1$ and is accompanied by a hyperbolic hedgehog defect of opposite topological charge ($s = −1$). The director field $\mathbf{n}(\mathbf{r})$ surrounding an elastic dipole at small distances is tilted away from $\mathbf{n}_0$ (Figure 1a). This tilt is represented by a two-dimensional polar vector $\mathbf{c}$ defined as a projection of the thickness-averaged $\mathbf{n}(\mathbf{r})$ onto the $x−y$ plane

and sketched with the help of "nail" symbols in Figure 1b. The tilt of $\mathbf{n}(\mathbf{r})$ around SP results in a radial distribution of $\mathbf{c}$ (Figure 1b), and under crossed polarizers, elastic dipoles in a homeotropic cell are seen as SP surrounded by four bright lobes separated by dark regions where $\mathbf{c}$ at the SP's perimeter matches the orientation of either the polarizer or the analyzer (Figure 1c). Using a full wave (λ = 530 nm) phase retardation plate with a slow axis γ placed after the sample at 45° between crossed polarizers, one can determine the orientation of $\mathbf{c}$ in a plane of the cell based on the interference colors in experimental micrographs. Interference colors in a LC texture are blue or yellow at non-zero $\mathbf{c} \| \gamma$ or $\mathbf{c} \perp \gamma$, respectively. Magenta color is seen in the regions where a non-zero $\mathbf{c}$ is parallel to either a polarizer or an analyzer or where $\mathbf{n}(\mathbf{r}) = \mathbf{n}_0$ and $\mathbf{c} = 0$.

Typically, a vertical position of colloidal inclusions in LC cells is determined by the balance between elastic repulsion from the walls of the confining substrates and gravitational force $F_g = (4/3)\pi R_0^3 \Delta \rho g \approx 0.26$ pN, where $\Delta \rho \approx 1650$ kg m^{-3} is the difference between LC and silica densities and $g = 9.8$ m s^{-2} is gravitational acceleration. In our case, due to the tight confinement, the vertical position of SPs is determined mainly by elastic repulsion from the walls as the force of this elastic repulsion can reach tens of piconewtons[12] and the modestly small contribution of F_g can be neglected. Due to the asymmetry of the dipolar configuration of $\mathbf{n}(\mathbf{r})$ distortions

with respect to the particle's equator, the elastic repulsion potential between an elastic dipole and a wall with homeotropic anchoring when a hedgehog is facing a wall is larger[27] by $\delta E_{wall} = 3\pi K\alpha\beta R_0^5 d^{-4}$, where K is an average elastic constant of a nematic LC and α and β are parameters related to dipole and quadrupole elastic moments,[22] respectively. Using $K \approx 12.7$ pN for ZLI-2806 and $\alpha \approx 2$ and $\beta \approx 0.5$ (refs 22, 28−30), we find the difference $\delta E_{wall} \approx 5000 k_B T$ for our case, where k_B is the Boltzmann constant and T is the temperature. Therefore, centers of mass of SPs do not reside perfectly in the middle of the cell but are slightly displaced by ≤ 0.5 μm toward one of the substrates; the particle's pole that is the closest to a hedgehog is pushed from a nearest wall farther away than another pole (Figure 1a).

At no electric fields applied to a LC cell, SPs are freely roaming in a plane of a cell due to Brownian motion (Figure 1d); displacements are independent of the in-plane direction (Figure 1e). The significant vertical displacements of SPs are prevented by a tight confinement in a very narrow gap. Even two-dimensional displacements of SPs in the plane of the cell are hindered by such tight confinement and strong elastic coupling with both substrates. A two-dimensional diffusion coefficient $D = 3.81 \times 10^{-4}$ μm^2 s^{-1} for SPs determined from their Brownian motion[1,31] (Figure 1f) in our thin cells was ∼3 times smaller than a diffusion coefficient $D = 12.65 \times 10^{-4}$ μm^2 s^{-1} of the same particles but in a 10 μm thick cell (Figure 1f) and almost 5 times smaller than a diffusion coefficient $D_{calc} = 18.7 \times 10^{-4}$ μm^2 s^{-1} in an isotropic phase calculated for a defect-free SP moving in an isotropic liquid with a viscosity $\eta = 75$ mPa s of LC using the Stokes−Einstein relation[1] $D_{calc} = k_B T/6\pi\eta R_0$. This indicates the strong role played by defects and elastic coupling of $\mathbf{n}(\mathbf{r})$ distortion fields around SPs to confining substrates, consistent with previous works of Stark,[32,33] Poulin,[31] and others[34−39] and even further demonstrating the role of confinement.

Electric-Field-Induced Colloid-Umbilic Topological Dipole. In our experiments, we used a nematic LC with a negative dielectric anisotropy $\Delta\varepsilon = -4.8$ so that the director $\mathbf{n}(\mathbf{r})$ orients orthogonally to an applied electric field. When an alternating current (ac) voltage U (Figure 2a) that is larger than a threshold voltage $U_{th} = \pi(K_3/\varepsilon_0|\Delta\varepsilon|)^{1/2}$, where K_3 is a bend Frank elastic constant, is applied to ITO electrodes (Figure 2b), the director far from the particle rotates from its initial homeotropic orientation to a tilted or even planar orientation depending on the voltage value because of LC's negative dielectric anisotropy (note that the deformation of the director corona around the particle is threshold-free and takes place even at very small voltages). The macroscopically homogeneous direction of the $\mathbf{n}(\mathbf{r})$ tilt and the corresponding $\mathbf{c}$ is predetermined by a small (1−2°) pretilt with respect to homeotropic alignment induced by a weak rubbing[40] along $\mathbf{e}_{r,t} \neq \mathbf{e}_{r,b}$ (Figures 1a and 2b). The director $\mathbf{n}(\mathbf{r})$ tilts in the direction of rubbing $\mathbf{e}_r$ (Figure 2b) as was confirmed by means of conoscopic observations.[41,42]

Panels e and g of Figure 2 show textures corresponding to the dynamics of $\mathbf{n}(\mathbf{r})$ configurations around an elastic dipole upon application of an electric field. Let us consider, for example, the SP closer to the bottom substrate (top schematic of Figure 2b). An applied voltage $U > U_{th}$ causes a homogeneous tilt of $\mathbf{n}(\mathbf{r})$ in the cell with respect to the amplitude of U and rubbing $\mathbf{e}_{r,b}$ with the in-plane $\mathbf{c}$ in the cell far from SPs oriented along $\mathbf{e}_{r,b}$. However, $\mathbf{n}(\mathbf{r})$ around the SP is already tilted away from $\mathbf{n}_0$ even before the application of

voltage because of homeotropic boundary conditions at a particle's surface (Figure 1a), and this tilt is radially symmetric with respect to $\mathbf{n}_0$, resulting in a radial $\mathbf{c}$ around SP (Figure 1b) with the direction of a polar $\mathbf{c}$ director in a $z-\mathbf{e}_{r,b}$ plane being opposite on the left and right side of SP. When a moderate voltage is applied, the magnitude of this preexisting tilt changes according to the strength of an electric field, but it does not change its direction with respect to the z axis as there is no preference in the azimuthal orientation of the tilt. Therefore, at one side of an elastic dipole along $\mathbf{e}_{r,b}$, $\mathbf{n}(\mathbf{r})$ is tilted in the direction opposite to overall tilt in the cell (Figure 2b). This mismatch in tilt and corresponding $\mathbf{c}$ directions in the cell and around an elastic dipole result in the appearance of a defect with four dark brushes in front of an elastic dipole with three of them closing on the surface of a particle (Figure 2d,e,g). These defects are umbilics,[2,43] regions where $\mathbf{c}$ rotates by 2π (Figure 2d), caused by the rotational degeneracy of the director tilt around an elastic dipole. The director field $\mathbf{n}(\mathbf{r})$ is continuous everywhere within an umbilic, and there are no singularities. Umbilics have a continuous effective core with a radius[43] $r_c \sim (d/\pi)[U_{th}^2/(U^2 - U_{th}^2)]^{1/2}$. When $U < U_{th}$, the core of umbilics spreads out and the originally spatially localized umbilic becomes undefined (Figure 1a). The umbilic's continuously deformed core contracts into a small region where four dark brushes meet (Figure 2c−e) when $U > U_{th}$, and r_c can be determined from the optical microscopy textures. The detailed $\mathbf{c}$-field around the colloid-umbilic pair (Figure 2d) can be deduced from polarizing optical microscopy textures using an additional retardation plate (Figure 2e,g). When $U > U_{th}$, there are two integer-strength self-compensating defects in the two-dimensional (2D) in-plane $\mathbf{c}$-field: one of strength $k = -1$ within an umbilic and another one with a particle itself in its core topologically equivalent to a defect with strength $k = +1$ (Figure 2d). The topological defects in the $\mathbf{c}$-field are well pronounced when $U > U_{th}$ because the radial distribution of $\mathbf{c}$ around the elastic dipole formed by SP and the accompanying hedgehog must be embedded in the homogeneous $\mathbf{c}$-field caused by an applied U and predetermined by the rubbing direction.

The observed periodic transformations of $\mathbf{n}(\mathbf{r})$ deformations around SPs due to the applied voltage oscillating between minimum and maximum values are also interesting from the perspective of classification of elastic multipoles in nemato-statics.[25,26] At no voltage applied, the SP and corona of the surrounding $\mathbf{n}(\mathbf{r})$ deformations form a well-known isotropic or uniaxial elastic dipole[25,26] with $C_{\infty v}$ symmetry where $\mathbf{n}(\mathbf{r})$ deformations are radially symmetric with respect to a line parallel to $\mathbf{n}_0$ going through the center of SP and a hedgehog (Figure 1a). When voltage is applied and an umbilic defect appears in the vicinity of SP, the uniaxial dipole continuously transforms into a general biaxial (nonchiral) dipole of C_{1v} symmetry. This C_{1v} elastic dipole has a $z-\mathbf{e}_r$ vertical mirror plane describing the only remaining symmetry operation bringing the structure into itself, apart from the trivial operations, like the 360° rotation (Figure 2b,c). This biaxial elastic dipole combines symmetry breaking along directions of the cell normal and in the plane of the cell along the rubbing directions. From the point of view of topology, the structures of the colloid-hedgehog dipole in $\mathbf{n}(\mathbf{r})$ and colloid-umbilic dipole in a 2D vector-field structure of $\mathbf{c}$ are consistent with topological charge conservation laws associated with the defect being embedded in uniform three-dimensional (3D)- and 2D-field backgrounds, respectively, in a manner that complies with
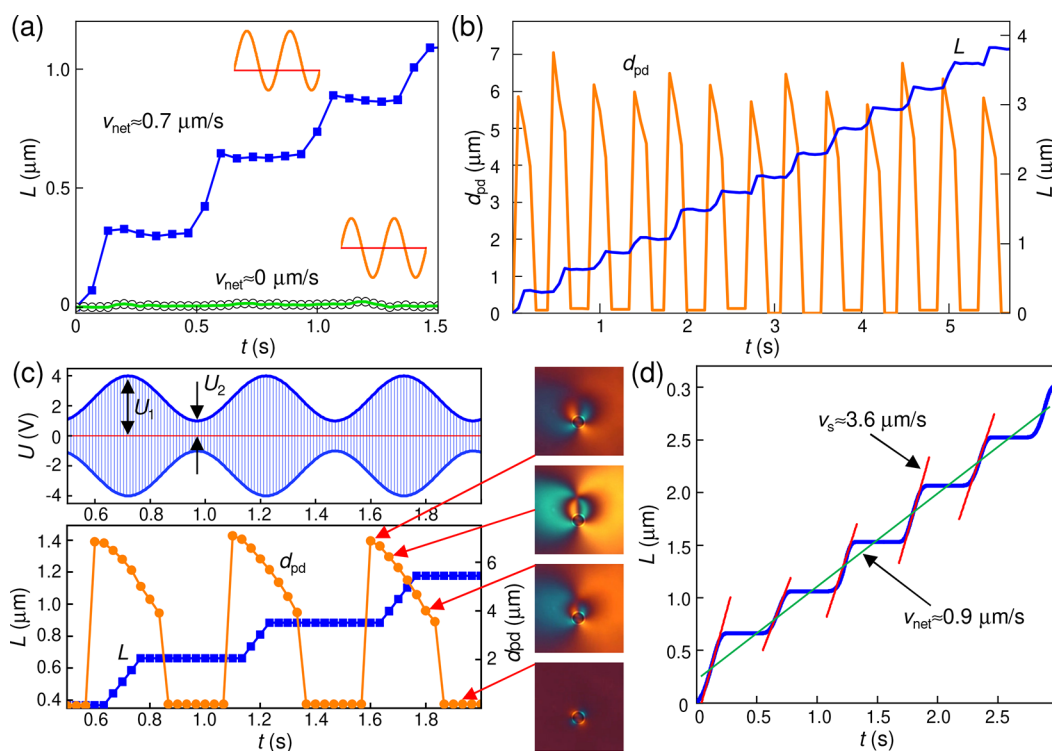
Figure 3. (a) Displacement of an elastic dipole over time at asymmetric and symmetric waveforms of the applied voltage. (b) Distance between an elastic dipole and an umbilic defect and corresponding displacement of an elastic dipole at $f_m = 2.25$ Hz. (c) Applied voltage waveform with $f_m = 2$ Hz and $f_c = 1$ kHz and corresponding distance between an elastic dipole and umbilic defect (orange filled circles) and displacement of an elastic dipole vs time (blue filled squares). Insets show corresponding $\mathbf{n(r)}$ textures obtained between crossed polarizers and a full wave retardation plate. (d) Plot of an elastic dipole's locomotion vs time (a blue line) showing details of stroke and net displacements. Red and green lines are linear fits for stroke and net displacements, respectively.

the constraints of topological theorems.[44] The configuration of the director field around the SP resembles that of a radial hedgehog and is a topologically nontrivial structure within the homotopy group $\pi_2(\mathbb{S}^2/\mathbb{Z}_2) = \mathbb{Z}$, compensated by a hyperbolic hedgehog belonging to the same homotopy class and having an elementary charge of an opposite sign (as one can see upon vectorizing the director[45]). In the 2D **c** director tilt vector field, the particle-induced and compensating field configurations belong to the first homotopy group, $\pi_1(\mathbb{S}^1) = \mathbb{Z}$, elements and self-compensate when embedded in the uniform far-field **c**. The interesting field-induced transformations reported here may find practical utility from the standpoint of new forms of controlled colloidal self-assembly.

Electric-Field-Driven Locomotion of Colloids. We used two waveforms of ac voltage in our experiments with the LC cells hosting elastic dipoles (Figure 2a). We applied either a sine-wave voltage at a low frequency $f_m = 1-5$ Hz or a square-wave with a high carrier frequency $f_c = 1$ kHz additionally modulated by a sine wave of a low frequency $f_m = 1-5$ Hz. The former waveform was also asymmetric with respect to a zero level due to our design that was based on combining it with a dc offset. In the latter waveform, having a high carrier frequency f_c allows us to avoid the effects associated with a transport of ions or ionic impurities at low-frequency applied electric fields and assuring only a dielectric response of LC. The important feature of used waveforms is that voltage magnitudes in each half-cycle are different so that $0 < U_2/U_1 < 0.5$ (Figures 2a and 3c). When an ac voltage of such waveforms is applied to the cells with elastic dipoles, they move in both lateral directions along $\mathbf{e}_r$ (Figure 2c) with the respective

change in the $\mathbf{n(r)}$ configurations around them (Figure 2e,g) that depends on f_m (Figure 2f). As mentioned above, due to the asymmetry of the 3D dipolar $\mathbf{n(r)}$ configuration, elastic dipoles are residing slightly closer to one of the substrates (Figure 1a). Thus, the vertical position of elastic dipoles in the cell and the particle-hedgehog dipole orientation of the elastic dipole moment determine not only the positions of induced umbilics but also the direction of translational motion of the particles. SPs effectively move in the direction of $\mathbf{e}_r$ at the nearest wall so that SP near the bottom substrate moves along $\mathbf{e}_{r,b}$ and SP near the top substrate moves along $\mathbf{e}_{r,t}$ (Figure 2b,c). The directional motion of elastic dipoles is stepwise (Figure 3a,b). The particle advances every half-cycle of the applied periodic voltage signal, when $U = U_1 > U_{th}$, and rests nearly motionless for another half-cycle when $U = U_2$ (Figures 2a and 3a,c). This jerky motion results in a net directional locomotion and displacement L of elastic dipoles with a net velocity $v_{net} > 0$ (Figure 3a). The asymmetry of an applied waveform with different voltage magnitudes $U_2 \neq U_1$ in each half-period is important for the efficient motion of elastic dipoles. Indeed, when a symmetrical sine wave voltage is applied, the net displacement of particles is equal to zero (Figure 3a).

During the first half-cycle of an oscillating signal, an amplitude of applied voltage is higher than the threshold value U_{th}, and an umbilic appears in front of the SP at some distance d_{pd} (Figure 2d) separated along $\mathbf{e}_{r,b}$. At first, the umbilic defect appears at the maximum distance (for a given modulation period) $d_{pd,max}$ from the SP (Figure 2d), which depends on the magnitude of the $\mathbf{n(r)}$ tilt caused by U. As the
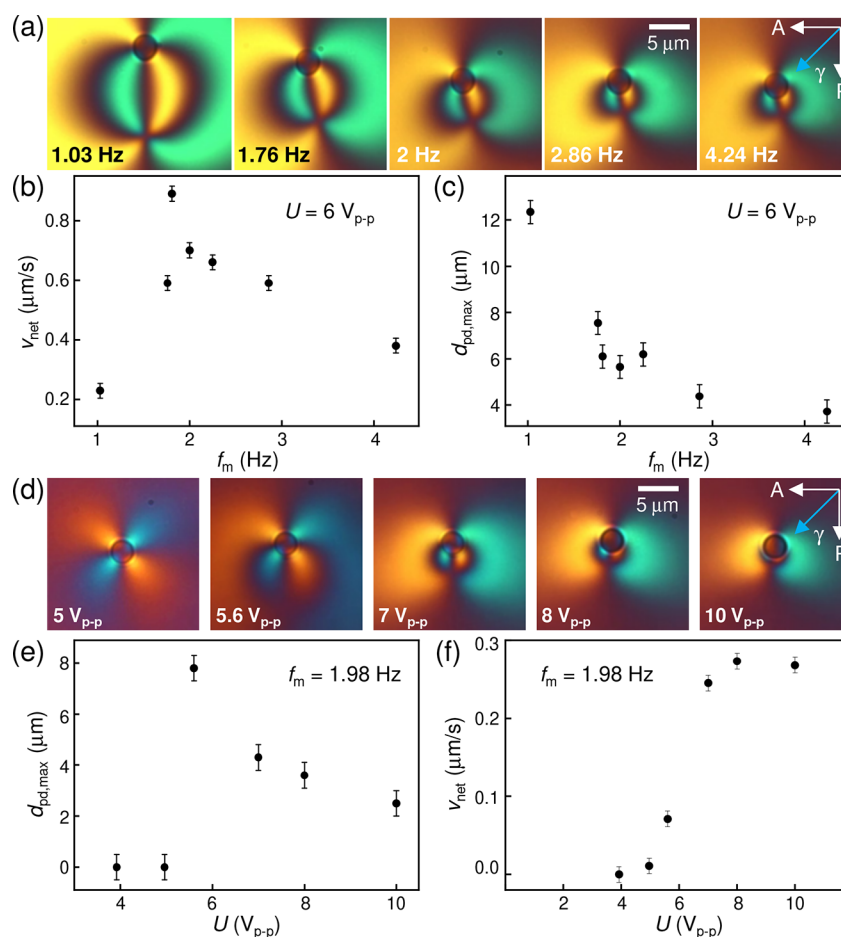
Figure 4. (a) Textures of $\mathbf{n(r)}$ obtained between crossed polarizers and a full wave retardation plate showing the distance $d_{\text{pd,max}}$ between an elastic dipole and umbilic defect depending on the frequency f_{m} of the applied voltage. (b) Velocity of SP and (c) distance $d_{\text{pd,max}}$ depending on the frequency f_{m} at a constant applied voltage $U = 6\ \text{V}_{\text{p-p}}$. (d) Textures of $\mathbf{n(r)}$ showing $d_{\text{pd,max}}$ between an elastic dipole and umbilic defect depending on the applied voltage at a constant frequency $f_{\text{m}} \approx 2$ Hz. (e) Distance $d_{\text{pd,max}}$ and (f) velocity v_{net} of SP depending on applied voltage at a constant frequency $f_{\text{m}} \approx 2$ Hz.

voltage signal evolves with time, the umbilic defect and colloidal SP particles move swiftly toward each other over a short period of time when $U > U_{\text{th}}$. Interestingly, the motion of SP does not continue all of the time while $U > U_{\text{th}}$ but only within a short period of time right before U reaches the maximum (Figure 3c), resulting in a jerky motion of a particle. The ensuing stepwise jerky displacement of the particle is directed along the particle-umbilic separation vector and repeats every other half-period, resulting, as time progresses, in a directional motion of the particle with some v_{net} (Figure 3b−d). Qualitatively, the temporal evolution of colloidal and director structures associated with the motion of an elastic dipole with accompanying dynamics of $\mathbf{n(r)}$ structure (Figure 3c and Video S1) resembles a swimmer moving with help of a butterfly stroke, albeit here this colloidal motion takes place at low Reynolds and Ericksen numbers and is possible primarily because of the nonreciprocity of the director-field evolution. Indeed, the temporal out-of-equilibrium evolutions of the director and $\mathbf{c}$-field distortions around particles with a voltage larger and smaller than U_{th} are not invariant upon reversal of time, as one can see from the polarizing optical micrograph sequences (Figure 2e,g), prompting lateral translations of SP in the nematic medium of a low Reynolds number. The particle's net period-averaged velocity can reach $v_{\text{net}} \approx 1\ \mu\text{m s}^{-1}$ depending on applied voltage parameters, but the instanta-

neous velocity v_{s} during each step or stroke is several times larger (Figure 3d); for example, when $U_1 = 4\ \text{V}_{\text{p-p}}$ at $f_{\text{m}} = 1.8$ Hz, the stroke velocity was measured to be $v_{\text{s}} \approx 3.6\ \mu\text{m s}^{-1}$. Key to the observed phenomena is the dynamics of the umbilical structure, which tends to localize at a well-defined distance from the SP within each modulation period and then interact with the SP at high instantaneous voltage magnitudes but spread smoothly at no applied field. At high instantaneous applied fields, the elastic dipole and umbilic are driven toward each other by elastic attraction forces between the corresponding topological defects of equal integer strength and opposite sign in the $\mathbf{c}$-field (Figure 2d), which minimizes their contribution to the free elastic energy. Experimentally measuring v_{s} and $D = 3.81 \times 10^{-4}\ \mu\text{m}^2\ \text{s}^{-1}$ for an elastic dipole (Figure 1b,d), one can determine a force F_{el} pulling on SP during elastic attraction between the umbilic and elastic dipole by balancing it with a viscous drag force $F_{\text{S}} = (k_{\text{B}}T/D)v_{\text{s}}$ as the Reynolds number $Re = \rho v_{\text{s}} R_0/\eta \approx 10^{-8} \ll 1$ at the LC density $\rho \approx 10^3\ \text{kg m}^{-3}$. The measured $F_{\text{el}} = 20−50$ pN is quite large and comparable to the magnitudes of forces of elastic attraction between elastic multipoles in nematics.[46−50] As a result of this elastic attraction, SPs are propelled by applied voltage in a well-defined direction along $\mathbf{e}_{\text{r}}$ (Figure 2c). Within the fractions of each modulation period when the instantaneous voltage is low or zero, the umbilic "spreads" to become a

delocalized structure of weak distortions that does not strongly interact with the SP. Thus, the nonreciprocity of director-field evolution with modulation can be also linked with and analyzed in terms of the asymmetry of elastic forces acting on the SP. From this direct experimental probing of elastic interactions between an elastic dipole and the induced umbilical structure, it is clear that the observed voltage-controlled directional motion of SP does not stem from hydrodynamic effects, electroconvection, backflows, or related phenomena involving the actual LC flows induced by fields; however, it certainly can be somewhat influenced by these effects, and flows are certainly generated by the particle as a consequence of its motion. Backflows associated with electric switching of the director cause negligible effects on the particle displacements as the elastic dipoles are held nearly in the middle of the cell due to the very tight confinement in a narrow cell gap almost comparable with the particle size. Unlike in the previous works on electrically driven and backflow-assisted particle motions,[15] our SPs are not substantially displaced from the cell middle toward substrates, where the nematic fluid displacement due to the backflow is maximized upon application of an electric field. Furthermore, the Ericksen number $Er = \eta v_s R_0 / K \approx 0.004-0.08$ at a LC viscosity $\eta \approx 1-300$ mPa s (covering typical values of LC's viscosity coefficients) is much smaller than unity, indicating that the flows do not couple strongly with the elastic deformations, as well as the dominance of elastic forces over the hydrodynamic forces[32,33,39] during the SP's locomotion.

To further elucidate any possible critical role that could be played by ionic currents and associated hydrodynamic effects, we used waveforms of applied voltage with a high carrier frequency $f_c = 1$ kHz (Figures 2a,f and 3c). The fact that the motion is found to be unimpeded when using this high carrier frequency shows that ionic effects are not critical for the observed phenomena. The high carrier frequency corresponds to electric-field direction oscillations and/or inversions within characteristic times $1/f_c$ short enough to preclude significant ion motions, supporting further the physical origins of the motion described above. The net velocity of elastic dipoles can be varied by varying a modulation frequency $f_m = 1-5$ Hz, a magnitude of applied voltage U, and $0.25 \leq U_2/U_1 < 0.5$ (Figure 4). The dependence of v_{net} on f_m or U is nonmonotonous (Figure 4b,f): v_{net} increases quadratically with U at a constant f_m but then quickly decreases after the applied voltage reaches modestly high values (>10 V_{p-p}), at which point the director in the middle plane of the cell is reoriented almost parallel to the substrates and an umbilic defect no longer appears in front of SP. At even higher applied voltages, the effectively immobile elastic dipole with typical $n(r)$ deformations[48-50] is observed in the nematic bulk with in-plane orientation of the far-field director across most of the cell thickness. Interestingly, there is a nonlinear correlation between v_{net} and a maximum distance between an elastic dipole and umbilic $d_{pd,max}$ upon its appearance, which decreases with an increase in either f_m or U (Figure 4a,c−e). It appears to be related to an optimal distance for elastic interactions between an elastic dipole and umbilic and their duration determined by the frequency of the applied voltage.

While our experiments provide insights into the importance of the nonreciprocal rotational dynamics of the director field in powering colloidal locomotion, the exact contributions and interplay of various effects in defining electrically driven nematic colloidal motions under different conditions in our experiments presented here and those in previous studies[13−19] will need to be explored further. For example, recently Long and Selinger have theoretically confirmed[51] that electric-field-induced motion of particle-like topological solitons can be explained by the nonreciprocal evolution of the director field, which is consistent with the earlier experimental and numerical findings.[20] Extensions of such theoretical models from purely solitonic-field configurations to the more complex case of nematic colloids could provide particularly valuable insights into the relative contributions of nonreciprocal director dynamics, elastic interactions, backflow, and electrokinetic and other effects in defining and controlling nematic colloidal locomotion under various experimental conditions.[13−19]

■ CONCLUSIONS

We have studied colloidal particles with homeotropic boundary conditions in thin homeotropic nematic cells and demonstrated electric-field-assisted formation of a dual-nature elastic/topological dipoles consisting of an always-present, conventional dipole of a colloid-hedgehog pair and a dynamically induced 2D topological dipole formed by a colloidal particle and an umbilic defect in the tilt directionality field. The nonreciprocal dynamics of a director-field transformation allows for electrically controlled locomotion of colloidal particles and can be analyzed in terms of LC-mediated interactions between the colloidal particle and an umbilic defect. We have shown that the dynamics of the director-field transformations depends on the amplitude and frequency of the applied voltage, with nonlinear dependencies of the velocity of locomotion of colloids on these parameters. Our results indicate that the nonreciprocal "squirming"-like evolution of particle-induced director structures and defects plays an important role in defining electrically powered dynamics and locomotion of colloidal particles in an oscillating field, similar to that also reported for topological solitons.[20,51] Our findings can be used to develop different driven, active, and other out-of-equilibrium self-reconfigurable systems, microfluidic transport systems, microrobotics,[52] and various technological applications. From a fundamental perspective, the described rich dynamic phenomena provide new insights into nematic colloids and their assembly, non-equilibrium reconfiguration behavior, and collective dynamics.

■ ASSOCIATED CONTENT

ⓈI Supporting Information

The Supporting Information is available free of charge at https://pubs.acs.org/doi/10.1021/acs.langmuir.1c02546.

Description of Video S1 (PDF)
Locomotion of a spherical colloidal particle with homeotropic boundary conditions in a vertically aligned nematic liquid crystal (AVI)

■ AUTHOR INFORMATION

Corresponding Author

Ivan I. Smalyukh − Department of Physics, Department of Electrical, Computer and Energy Engineering, Soft Materials Research Center and Materials Science and Engineering Program, and Chemical Physics Program, Departments of Chemistry and Physics, University of Colorado, Boulder, Colorado 80309, United States; Renewable and Sustainable Energy Institute, National Renewable Energy Laboratory and University of Colorado, Boulder, Colorado 80309, United

States; ⬤ orcid.org/0000-0003-3444-1966;
Email: ivan.smalyukh@colorado.edu

Authors

Bohdan Senyuk − *Department of Physics, University of Colorado, Boulder, Colorado 80309, United States*

Richmond E. Adufu − *Department of Electrical, Computer and Energy Engineering, University of Colorado, Boulder, Colorado 80309, United States*

Complete contact information is available at:
https://pubs.acs.org/10.1021/acs.langmuir.1c02546

Author Contributions

B.S. and R.E.A. conducted the experiments. I.I.S. conceived and directed the project. B.S. and I.I.S. analyzed the results. The manuscript was written through contributions of all authors. All authors have given approval to the final version of the manuscript.

Notes

The authors declare no competing financial interest.

◼ REFERENCES

(1) Chaikin, P. M.; Lubensky, T. C. *Principles of Condensed Matter Physics*; Cambridge University Press: Cambridge, U.K., 2000.
(2) de Gennes, P. G.; Prost, J. *The Physics of Liquid Crystals*; Clarendon: Oxford, U.K., 1995.
(3) Vicsek, T.; Zafeiris, A. Collective Motion. *Phys. Rep.* **2012**, *517*, 71−140.
(4) Marchetti, M. C.; Joanny, J. F.; Ramaswamy, S.; Liverpool, T. B.; Prost, J.; Rao, M.; Aditi Simha, R. Hydrodynamics of Soft Active Matter. *Rev. Mod. Phys.* **2013**, *85*, 1143−1189.
(5) Brown, A. T.; Vladescu, I. D.; Dawson, A.; Vissers, T.; Schwarz-Linek, J.; Lintuvuori, J. S.; Poon, W. C. K. Swimming in a Crystal. *Soft Matter* **2016**, *12*, 131−140.
(6) Simmchen, J.; Katuri, J.; Uspal, W. E.; Popescu, M. N.; Tasinkevych, M.; Sánchez, S. Topographical Pathways Guide Chemical Microswimmers. *Nat. Commun.* **2016**, *7*, 10598.
(7) Neta, P. D.; Tasinkevych, M.; Telo da Gama, M. M.; Dias, C. S. Wetting of a Solid Surface by Active Matter. *Soft Matter* **2021**, *17*, 2468−2478.
(8) Sohn, H. R. O.; Smalyukh, I. I. Electrically Powered Motions of Toron Crystallites in Chiral Liquid Crystals. *Proc. Natl. Acad. Sci. U.S.A.* **2020**, *117*, 6437−6445.
(9) Sohn, H. R. O.; Liu, C. D.; Smalyukh, I. I. Schools of Skyrmions with Electrically Tunable Elastic Interactions. *Nat. Commun.* **2019**, *10*, 4744.
(10) Smalyukh, I. I.; Kachynski, A. V.; Kuzmin, A. N.; Prasad, P. N. Laser Trapping in Anisotropic Fluids and Polarization-Controlled Particle Dynamics. *Proc. Natl. Acad. Sci. U.S.A.* **2006**, *103*, 18048−18053.
(11) Varney, M. C. M.; Zhang, Q.; Smalyukh, I. I. Stick-Slip Motion of Surface Point Defects Prompted by Magnetically Controlled Colloidal-Particle Dynamics in Nematic Liquid Crystals. *Phys. Rev. E* **2015**, *91*, 052503.
(12) Senyuk, B.; Varney, M. C. M.; Lopez, J. A.; Wang, S.; Wu, N.; Smalyukh, I. I. Magnetically Responsive Gourd-Shaped Colloidal Particles in Cholesteric Liquid Crystals. *Soft Matter* **2014**, *10*, 6014−6023.
(13) Lavrentovich, O. D. Active Colloids in Liquid Crystals. *Curr. Opin. Colloid Interface Sci.* **2016**, *21*, 97−109.

(14) Dierking, I.; Biddulph, G.; Matthews, K. Electromigration of Microspheres in Nematic Liquid Crystals. *Phys. Rev. E* **2006**, *73*, 011702.
(15) Pishnyak, O. P.; Tang, S.; Kelly, J. R.; Shiyanovskii, S. V.; Lavrentovich, O. D. Levitation, Lift, and Bidirectional Motion of Colloidal Particles in an Electrically Driven Nematic Liquid Crystal. *Phys. Rev. Lett.* **2007**, *99*, 127802.
(16) Jákli, A.; Senyuk, B.; Liao, G.; Lavrentovich, O. D. Colloidal Micro-Motor in Smectic A Liquid Drystal Driven by DC Electric Field. *Soft Matter* **2008**, *4*, 2471−2474.
(17) Mieda, Y.; Furutani, K. Two-Dimensional Micromanipulation Using Liquid Crystals. *Appl. Phys. Lett.* **2005**, *86*, 101901.
(18) Ryzhkova, A. V.; Podgornov, F. V.; Haase, W. Nonlinear Electrophoretic Motion of Dielectric Microparticles in Nematic Liquid Crystals. *Appl. Phys. Lett.* **2010**, *96*, 151901.
(19) Sahu, D. K.; Kole, S.; Ramaswamy, S.; Dhara, S. Omnidirectional Transport and Navigation of Janus Particles through a Nematic Liquid Crystal Film. *Phys. Rev. Res.* **2020**, *2*, 032009.
(20) Ackerman, P. J.; Boyle, T.; Smalyukh, I. I. Squirming Motion of Baby Skyrmions in Nematic Fluids. *Nat. Commun.* **2017**, *8*, 673.
(21) Poulin, P.; Stark, H.; Lubensky, T.; Weitz, D. Novel Colloidal Interactions in Anisotropic Fluids. *Science* **1997**, *275*, 1770−1773.
(22) Lubensky, T. C.; Pettey, D.; Currier, N.; Stark, H. Topological Defects and Interactions in Nematic Emulsions. *Phys. Rev. E* **1998**, *57*, 610−625.
(23) Poulin, P.; Weitz, D. A. Inverted and Multiple Nematic Emulsions. *Phys. Rev. E* **1998**, *57*, 626−637.
(24) Stark, H. Physics of Colloidal Dispersions in Nematic Liquid Crystals. *Phys. Rep.* **2001**, *351*, 387−474.
(25) Pergamenshchik, V. M.; Uzunova, V. A. Colloidal Nemato-statics. *Condens. Matter Phys.* **2010**, *13*, 33602.
(26) Pergamenshchik, V. M.; Uzunova, V. A. Dipolar Colloids in Nematostatics: Tensorial Structure, Symmetry, Different Types, and their Interaction. *Phys. Rev. E* **2011**, *83*, 021701.
(27) Chernyshuk, S. B.; Lev, B. I. Theory of Elastic Interaction of Colloidal Particles in Nematic Liquid Crystals Near One Wall and in the Nematic Cell. *Phys. Rev. E* **2011**, *84*, 011707.
(28) Noël, C. M.; Bossis, G.; Chaze, A.-M.; Giulieri, F.; Lacis, S. Measurement of Elastic Forces between Iron Colloidal Particles in a Nematic Liquid Crystal. *Phys. Rev. Lett.* **2006**, *96*, 217801.
(29) Takahashi, K.; Ichikawa, M.; Kimura, Y. Force between Colloidal Particles in a Nematic Liquid Crystal Studied by Optical Tweezers. *Phys. Rev. E* **2008**, *77*, 020703.
(30) Kishita, T.; Takahashi, K.; Ichikawa, M.; Fukuda, J.; Kimura, Y. Arrangement Dependence of Interparticle Force in Nematic Colloids. *Phys. Rev. E* **2010**, *81*, 010701.
(31) Loudet, J. C.; Hanusse, P.; Poulin, P. Stokes Drag on a Sphere in a Nematic Liquid Crystal. *Science* **2004**, *306*, 1525.
(32) Stark, H.; Ventzki, D. Stokes Drag of Spherical Particles in a Nematic Environment at Low Ericksen Numbers. *Phys. Rev. E* **2001**, *64*, 031711.
(33) Stark, H.; Ventzki, D.; Reichert, M. Recent Developments in the Field of Colloidal Dispersions in Nematic Liquid Crystals: the Stokes Drag. *J. Phys.: Condens. Matter* **2003**, *15*, S191.
(34) Koenig, G. M.; Ong, R.; Cortes, A. D.; Moreno-Razo, J. A.; de Pablo, J. J.; Abbott, N. L. Single Nanoparticle Tracking Reveals Influence of Chemical Functionality of Nanoparticles on Local Ordering of Liquid Crystals and Nanoparticle Diffusion Coefficients. *Nano Lett.* **2009**, *9*, 2794−2801.
(35) Ryzhkova, A. V.; Muševič, I. Particle Size Effects on Nanocolloidal Interactions in Nematic Liquid Crystals. *Phys. Rev. E* **2013**, *87*, 032501.
(36) Moreno-Razo, J. A.; Sambriski, E. J.; Koenig, G. M.; Diaz-Herrera, E.; Abbott, N. L.; de Pablo, J. J. Effects of Anchoring Strength on the Diffusivity of Nanoparticles in Model Liquid-Crystalline Fluids. *Soft Matter* **2011**, *7*, 6828−6835.
(37) Sanders, J. L.; Yang, Y.; Dickinson, M. R.; Gleeson, H. F. Pushing, Pulling and Twisting Liquid Crystal Systems: Exploring New

Directions with Laser Manipulation. *Philos. Trans. R. Soc. A* **2013**, *371*, 20120265.

(38) Senyuk, B.; Glugla, D.; Smalyukh, I. I. Rotational and Translational Diffusion of Anisotropic Gold Nanoparticles in Liquid Crystals Controlled by Varying Surface Anchoring. *Phys. Rev. E* **2013**, *88*, 062507.

(39) Fukuda, J.; Stark, H.; Yoneya, M.; Yokoyama, H. Dynamics of a Nematic Liquid Crystal around a Spherical Particle. *J. Phys.: Condens. Matter* **2004**, *16*, S1957.

(40) Sinha, G. P.; Wen, B.; Rosenblatt, C. Large, Continuously Controllable Nematic Pretilt from Vertical Orientation. *Appl. Phys. Lett.* **2001**, *79*, 2543−2545.

(41) Van Horn, B. L.; Winter, H. H. Analysis of the Conoscopic Measurement for Uniaxial Liquid-Crystal Tilt Angles. *Appl. Opt.* **2001**, *40*, 2089−2094.

(42) Senyuk, B.; Wonderly, H.; Mathews, M.; Li, Q.; Shiyanovskii, S. V.; Lavrentovich, O. D. Surface Alignment, Anchoring Transitions, Optical Properties, and Topological Defects in the Nematic Phase of Thermotropic Bent-Core Liquid Crystal A131. *Phys. Rev. E* **2010**, *82*, 041711.

(43) Rapini, A. Umbilics: Static Properties and Shear-Induced Displacements. *J. Phys. (Paris)* **1973**, *34*, 629−633.

(44) Smalyukh, I. I. Liquid Crystal Colloids. *Annu. Rev. Condens. Matter Phys.* **2018**, *9*, 207−226.

(45) Senyuk, B.; Liu, Q.; He, S.; Kamien, R. D.; Kusner, R. B.; Lubensky, T. C.; Smalyukh, I. I. Topological Colloids. *Nature* **2013**, *493*, 200−205.

(46) Smalyukh, I. I.; Kuzmin, A. N.; Kachynski, A. V.; Prasad, P. N.; Lavrentovich, O. D. Optical Trapping of Colloidal Particles and Measurement of the Defect Line Tension and Colloidal Forces in a Thermotropic Nematic Liquid Crystal. *Appl. Phys. Lett.* **2005**, *86*, 021913.

(47) Smalyukh, I. I.; Lavrentovich, O. D.; Kuzmin, A. N.; Kachynski, A. V.; Prasad, P. N. Elasticity-Mediated Self-Organization and Colloidal Interactions of Solid Spheres with Tangential Anchoring in a Nematic Liquid Crystal. *Phys. Rev. Lett.* **2005**, *95*, 157801.
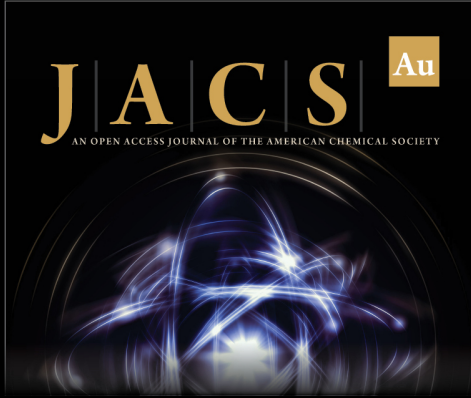
(48) Škarabot, M.; Ravnik, M.; Žumer, S.; Tkalec, U.; Poberaj, I.; Babič, D.; Osterman, N.; Muševič, I. Two-Dimensional Dipolar Nematic Colloidal Crystals. *Phys. Rev. E* **2007**, *76*, 051406.

(49) Kishita, T.; Kondo, N.; Takahashi, K.; Ichikawa, M.; Fukuda, J.; Kimura, Y. Interparticle Force in Nematic Colloids: Comparison between Experiment and Theory. *Phys. Rev. E* **2011**, *84*, 021704.

(50) Martinez, A.; Mireles, H. C.; Smalyukh, I. I. Large-Area Optoelastic Manipulation of Colloidal Particles in Liquid Crystals Using Photoresponsive Molecular Surface Monolayers. *Proc. Natl. Acad. Sci. U.S.A.* **2011**, *108*, 20891−20896.

(51) Long, C.; Selinger, J. V. Coarse-Grained Theory for Motion of Solitons and Skyrmions in Liquid Crystals. *Soft Matter* **2021**, *17*, 10437.

(52) Liu, Q.; Wang, W.; Reynolds, M. F.; Cao, M. C.; Miskin, M. Z.; Arias, T. A.; Muller, D. A.; McEuen, P. L.; Cohen, I. Micrometer-Sized Electrically Programmable Shape-Memory Actuators for Low-Power Microrobotics. *Science Robotics* **2021**, *6*, eabe6663.